HAL open science

BODIPY-loaded polymer nanoparticles: chemical structure of cargo defines leakage from nanocarrier in living cells

Kateryna Trofymchuk, Jurga Valanciunaite, Bohdan Andreiuk, Andreas Reisch, Mayeul Collot, Andrey S Klymchenko

To cite this version:

Kateryna Trofymchuk, Jurga Valanciunaite, Bohdan Andreiuk, Andreas Reisch, Mayeul Collot, et al.. BODIPY-loaded polymer nanoparticles: chemical structure of cargo defines leakage from nanocarrier in living cells. Journal of materials chemistry B, 2019, 7 (34), pp.5199-5210. 10.1039/C8TB02781A . hal-02383707

HAL Id: hal-02383707

https://hal.science/hal-02383707v1

Submitted on 31 Jan 2020

HAL is a multi-disciplinary open access archive for the deposit and dissemination of scientific research documents, whether they are published or not. The documents may come from teaching and research institutions in France or abroad, or from public or private research centers.

L'archive ouverte pluridisciplinaire **HAL**, est destinée au dépôt et à la diffusion de documents scientifiques de niveau recherche, publiés ou non, émanant des établissements d'enseignement et de recherche français ou étrangers, des laboratoires publics ou privés.

BODIPY-loaded polymer nanoparticles: chemical structure of cargo defines leakage from nanocarrier in living cells

Kateryna Trofymchuk, Jurga Valanciunaite, Bohdan Andreiuk, Andreas Reisch, Mayeul Collot,* and Andrey S. Klymchenko*

Nanochemistry and Bioimaging group, Laboratoire de Bioimagerie et Pathologies, UMR 7021 CNRS, Université de Strasbourg, 74 route du Rhin, 67401, Illkirch, France

*Corresponding authors: andrey.klymchenko@unistra.fr; mayeul.collot@unistra.fr

Abstract

Uncontrolled release of encapsulated drugs and contrast agents from biodegradable polymer nanoparticles (NPs) is a central problem in drug delivery and bioimaging. In particular, it concerns polymeric NPs prepared by nanoprecipitation, where this release (so-called burst release) can be very significant, leading to side effects and/or bioimaging artifacts. Here, we made a systematic study on the effect of chemical structure of cargo molecules, BODIPY dye derivatives, on their capacity to be loaded into ~50 nm PLGA NPs without leakage in biological media. Absorption and fluorescence spectroscopy suggested that most of dyes, except the most polar BODIPY derivative, formed blended structures with polymer NPs. Fluorescence correlation spectroscopy of dye-loaded NPs in the presence of serum proteins revealed that only the most hydrophobic BODIPY dyes, bearing one octadecyl chain or two octyl chains, remain inside NPs, while all other derivatives are released into serum medium. The time-laps absorption and fluorescence studies confirmed this result, suggesting the release kinetics for the leaky NPs on the time scale of hours. Fluorescence microscopy of living cells incubated with BODIPY-loaded NPs showed that most of them exhibit strong dye leakage observed as homogeneous distribution of fluorescence all over the cytoplasm. Importantly, NPs loaded with the most hydrophobic dyes, exhibited high stability showing a dotted pattern in the perinuclear region, typical for endosomes and lysosomes. Our results highlight significance of the cargo hydrophobicity for efficient encapsulation inside polymeric NPs prepared by nanoprecipitation, which enables designing stable cargo-loaded nanomaterials for bioimaging and drug delivery.

Introduction

The primary feature of nanoparticles (NPs) as tools for nanomedicine is their capacity to encapsulate a cargo, as it enables targeted delivery of drugs or contrast agents to the cells and tissues preventing non-specific distribution of active molecules all over the body.[1-3] Polymer NPs are particularly promising nanocarriers, because their solid hydrophobic matrix can efficiently host a variety of hydrophobic guest molecules, in particular drugs.[4, 5] As polymer NPs can be built from biodegradable matrix polymers, the nanocarrier can be cleared from the body and ensure long-term release of active molecules.[6-8] One of the major limitations of these nanocarriers is uncontrolled rapid leakage (or leaching) of the cargo in biological media, also called burst release. [9-14] It results in undesired release of drugs in healthy tissues producing toxic side effects. One reason for burst release is related to matrix properties of polymer NPs, in particular porosity, which favors fast diffusion of the drug within the matrix towards the NP surface.[10, 15, 16] The other key reason is surface adsorption of the cargo instead of its encapsulation inside the matrix of the NP. Uncontrolled rapid release is particularly critical in biological media and cells, because hydrophobic cargo, being insoluble in water can be readily solubilized by lipid components of serum or cell membranes. As release of drugs is very difficult to monitor in complex biological media and in live cells, fluorescent dyes are used as model cargos for polymer NPs.[17-23]

Dye-loaded polymeric NPs are attractive systems to address the problem of cargo leakage. On one hand, they are powerful tools for fluorescence bioimaging in vitro and in vivo.[24-26] Indeed, owing to high brightness, biodegradability and capacity to encapsulate different cargos, dye-loaded polymer NPs emerged as a powerful alternative to inorganic nanoparticles, such as quantum dots,[27, 28] dye-doped silica NPs,[29, 30] etc. They have already found a variety of applications, including cellular and *in vivo* imaging,[31, 32], imaging of cellular uptake,[33-36] long-term cell tracking,[24, 35] cell barcoding,[24] receptor-specific cell targeting,[31, 37, 38] single-molecule detection[39] and single-particle tracking[40], biosensing,[41] as well as *in vivo* studies for visualizing tumors[42, 43], theranostics[44], photodynamic therapy,[45] etc. On the other hand, dye-loaded polymeric NPs can model the behavior of drug-loaded NPs. The encapsulated fluorescent dyes are excellent probes that can report on the cargo release from nanocarriers.[17-23] Dye-loaded and drug-loaded NPs share two key common requirements. The first requirement is the high loading of cargo. In drug-loaded NPs, it is essential for enhancing therapeutic efficacy, whereas in dye-loaded NPs, it is needed to reach the maximal possible brightness. However, in dye-loaded NPs, high loading leads to aggregation-caused quenching (ACQ), because of π-stacking of flat aromatic dye molecules into non-fluorescent *H*-aggregates. Several methods have been developed to date to prevent ACQ: aggregation-induced emission [46], the use of bulky side groups[47, 48] and bulky hydrophobic counterions [33, 49]. Secondly, similarly to drug-loaded NPs, dye-loaded NPs should be stable against rapid cargo leakage inside biological systems. Indeed, the liberated dye of NPs is a source of strong background and non-specific off-target fluorescence. In this case, the cells incubated with NPs become strongly fluorescent not because of the nanoparticle entry, but due to leakage of dyes from particles in solution and their further diffusion inside cells.[17-19, 22, 50] Some reports linked the problem of dye leakage to insufficient hydrophobicity of the encapsulated dyes.[19, 21] However, so far there is no systematic study on the importance of chemical structure of cargo dye for preventing the burst release in biological media and living cells.

In the present work, we synthesized various BODIPY dye derivatives bearing different hydrophobic groups: aromatic as well as aliphatic groups with single or multiple hydrocarbon chains. BODIPYs are neutral dyes with low polarity, featuring excellent absorption and fluorescent properties.[51, 52] BODIPY

dyes and their analogues have been attractive building blocks in molecular and nano-constructs for fluorescence imaging and photodynamic therapy applications.[53-57] Therefore, they are good candidates as a model cargo. Using the biodegradable polymer poly(lactic-co-glycolic acid) (PLGA), we prepared NPs by nanoprecipitation containing different BODIPY derivatives. NPs were characterized depending on the BODIPY structure and loading concentration by measuring their size, aggregation of dyes inside NPs and fluorescence quantum yield. Then, using florescence correlation spectroscopy (FCS) we evaluated the leakage of different BODIPY dyes from NPs in the presence of fetal bovine serum (FBS). Finally, the stability of NPs loaded with different BODIPY dyes was tested after incubation with living Hela cells by confocal fluorescence microscopy.

Results and discussion

As parent compounds, we selected B-P and B-Mes, where the latter bears additional ethyl groups in the β position pyrrole rings and a mesityl group at the *meso* position, instead of phenyl. In addition to higher hydrophobicity of B-Mes, these additional groups were reported to decrease aggregation-caused quenching of the dyes.[58] Based on core structure of B-Mes, we designed a series of BODIPY derivatives, where aryl group at *meso* position was replaced with different hydrophobic groups. To this end, a corresponding BODIPY-acid derivative 1 was synthesized, which was further reacted with different primary and secondary aliphatic amines to afford final hydrophobic BODIPY derivatives (Scheme 1).

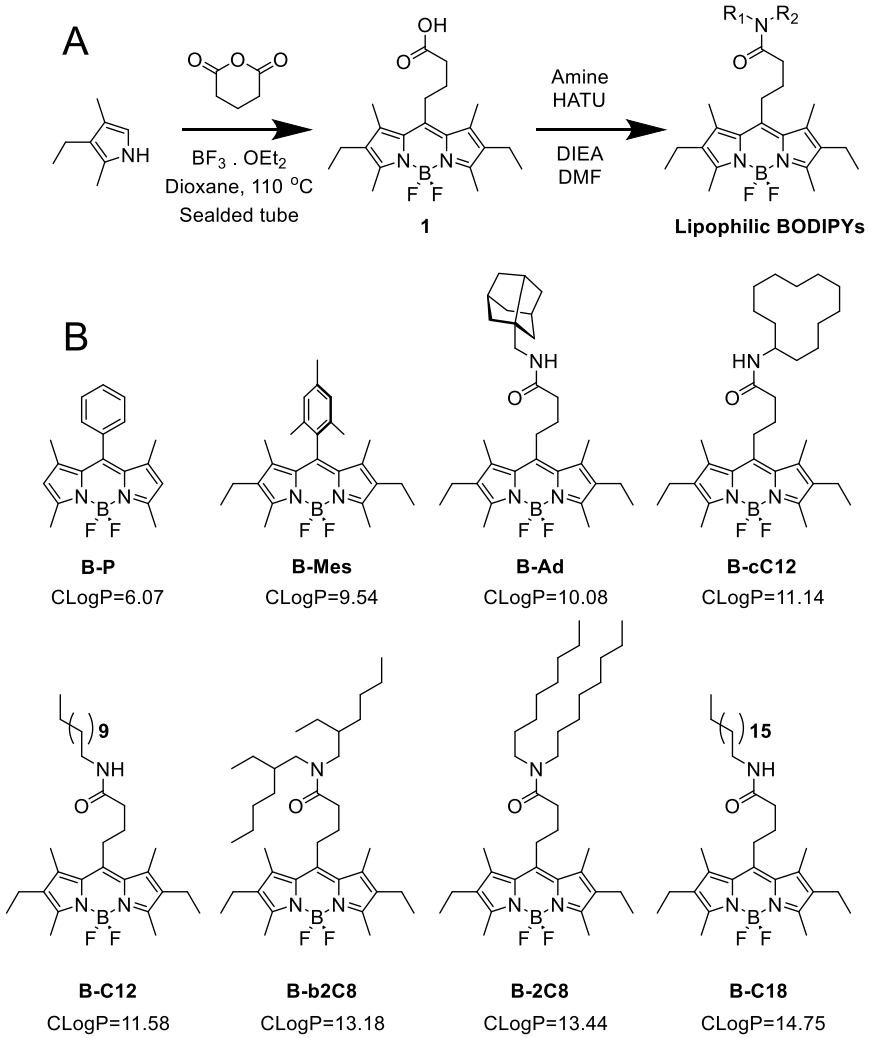

Scheme 1. (A) Synthesis of the hydrophobic BODIPYs. (B) Chemical structures of studied BODIPY dye derivatives and their calculated LogP (CLogP) values denoting their increasing lipophilicity.

Further, we have prepared blended PLGA-BODIPY NPs containing different amounts of BODIPY dyes using our previously developed nanoprecipitation method.[33, 59] It is based on solvent displacement,[60] but in our case the use of hydrophobic polymer bearing one charged group per polymer enables preparation of relatively small NPs in the size range (15-60 nm).[33, 59] In the present case, a solution of PLGA and a corresponding BODIPY dye in acetonitrile was injected rapidly into aqueous buffer under intense shaking at rt. The obtained NPs were studied without further purification, because neither dialysis nor filtration through a hydrophobic (PTFE) filter changed the dye concentration in the sample (data not shown). Owing to spherical shape of dye-loaded PLGA NPs prepared by nanoprecipitation,[24, 59] their size can be characterized by dynamic light scattering (DLS). Figure 1A shows the hydrodynamic diameters of the produced BODIPY-loaded polymer NPs. At dye loadings ≤ 200 mM (with respect to the polymer), the hydrodynamic diameter of most BODIPY NPs was about 35-40 nm. At 200 mM dye loading and higher, the size of all BODIPY NPs increased to 45-60 nm. BODIPY NPs displayed quite narrow volume size distribution (e.g. polydispersity index (PDI) 0.068-0.192 for NPs with 100 mM loading) with a single maximum that was shifted slightly to higher values with increase in the dye loading (Fig. S1). It should be noted, that the size of produced BODIPY-loaded polymer NPs was 4 to 5 times lower than that of BODIPY aggregates formed in the same aqueous buffer without the polymer, using concentration corresponding to 100 mM loading (Fig. 1B). Interestingly, BODIPY aggregates also displayed a mono-modal size distribution, however the distribution curves were broader (PDI 0.086-0.27) in comparison to PLGA NPs at corresponding dye concentration (Fig. S1). Formation of monodisperse NPs have been previously shown for some hydrophobic dyes.[61, 62] Significantly smaller size of NPs than that of aggregates suggests that during nanoprecipitation hydrophobic BODIPY dyes form blended structures with PLGA NPs.

To estimate the fraction of the dye that was blended with NPs, i.e. the loading efficiency, we used PTFE filter of 200 nm, which was expected to separate dye-loaded NPs from dye aggregates in water. In a control experiment, the filtration of dye NPs prepared without PLGA resulted in nearly complete disappearance of the dye absorption, as shown from the UV-visible spectra (Fig. S2). This result is in line with the large size of the dye aggregates without polymer (Fig. 1B). In a sharp contrast, after filtration of dye-loaded PLGA NPs, a large fraction of the dye was still observed in the absorption spectra (Fig. 1C and Fig. S2). These results suggest the filtration process could separate to some extent the dye-loaded polymeric NPs from dye aggregates in water, so that the fraction the dye in the filtered NPs with respect to total dye before the filtration reflects the dye loading efficiency (Fig. 1C). Remarkably, nearly all tested BODIPYs showed high dye loading efficiency, around 90%, except the least hydrophobic B-P showing 73.4±0.5 % efficiency. Based on the feeding ratio dye/polymer, the encapsulation efficiency, and measured hydrodynamic diameter of NPs, the number of dyes per particle can be theoretically estimated. For instance, in case of B-2C8 at 200 mM loading (86.1 % loading efficiency, 50 nm diameter), the estimated number of dyes per particle is ~6800.

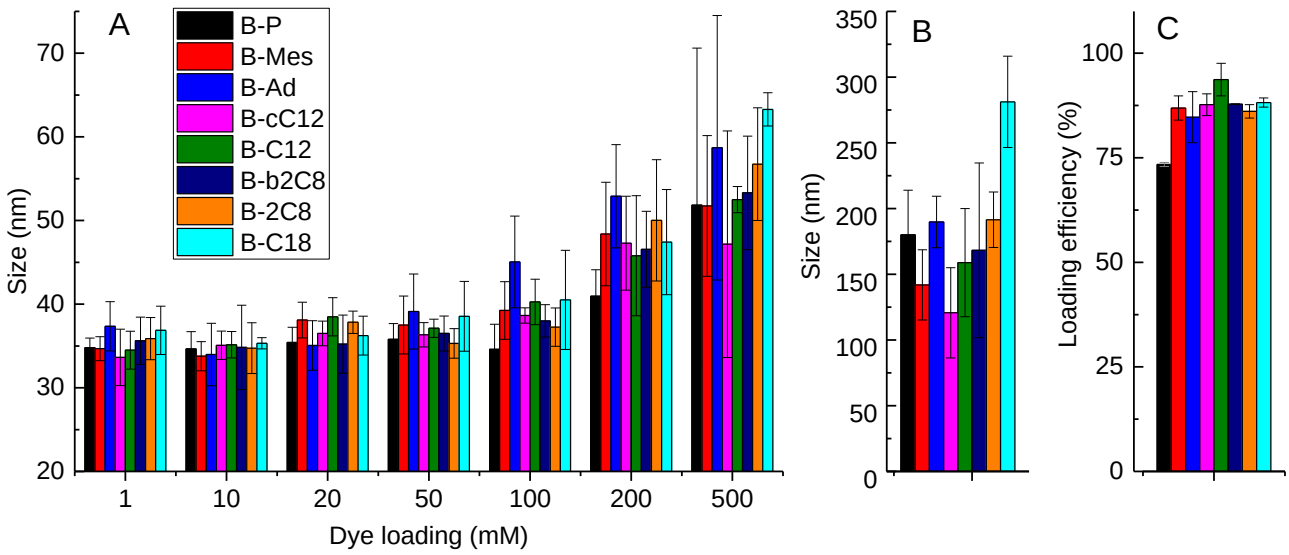

Figure 1. Hydrodynamic diameters of PLGA NPs encapsulating different BODIPY dyes at various loadings measured by DLS (A). Samples without polymer (in buffer) (B) were prepared in the same way as NP solutions, using concentration corresponding to 100 mM loading. 20 mM phosphate buffer (pH 7.4) was systematically used. The size analysis was based on the statistics by volume. Loading efficiency of different BODIPY dyes in PLGA NPs calculated from UV- visible absorbance changes after filtration through PTFE filter (C). The formulation corresponds to 200 mM dye loading.

The absorption and fluorescence spectra of representative NPs loaded with different amounts of B-Mes, and more hydrophobic B-C18, bearing the longest hydrophobic chain, are shown in Figure 2. In the organic solvent methanol, where only molecular species of BODIPY dyes are expected, the absorption spectrum displayed a single band at 520 nm with a slight shoulder on the blue side for both dyes (Fig. 2). On the other hand, in water, where these dyes are poorly soluble, the absorption spectra of both dyes showed significant broadening with a shoulder at the shorter wavelengths, which, according to early works is a characteristic to formation of aggregated species.[63] At the lowest studied loadings in PLGA NPs (1 mM), BODIPY dyes displayed absorption spectra typical for non-aggregated dyes, like in methanol, although for B-C18 a small short-wavelength shoulder of aggregates could already be noticed. At high dye BODIPY loading (200 mM), a strong broadening of absorption spectra and an increase in the shoulder were observed for all studied dyes (Fig. 2, 3 and S3), indicating that BODIPY dyes tend to form aggregates in PLGA NPs. Nevertheless, B-C18 displayed stronger tendency to aggregate in PLGA matrix than B-Mes, as the characteristic short-wavelength shoulder was observed for B-C18 at low and medium loadings, in contrast to B-Mes (Fig. 2). When all synthesized dyes were compared together using the absorbance ratio at the shoulder *vs* the maximum (Fig. 3), it can be seen that aggregation in polymer NPs was much more pronounced for BODIPY dyes with long and branched hydrophobic chains, such as B-C18, B-C12 and B-2C8, B-b2C8. The least aggregated was B-P dye, which is clearly the least hydrophobic one. BODIPY dyes bearing cyclic groups, B-Ad and B-cC12, showed intermediate aggregation inside PLGA NPs. In any case, even at 200 mM loading the absorption spectra of dyes in PLGA NPs were narrower than those in water without polymer (Fig. 2 and S3), which additionally support that the dyes are blended with PLGA in particles.

Fluorescence spectra reflected similar tendencies. The emission spectra of B-Mes and B-C18 were narrow in methanol, whereas in water they were much broader and red-shifted (Fig. 2). When co-precipitated with PLGA NPs at low dye loading, they showed emission spectra similar to that in methanol, indicating that majority of emissive species are in the molecular form within PLGA polymer matrix. However, at higher loadings, broadening of the emission band together with the red shift was observed for both dyes (Fig. 2) as well as for all other studied BODIPY derivatives (Fig. S4). These spectral changes indicate that aggregation of BODIPY molecules in polymer NPs occurs at high dye loadings.

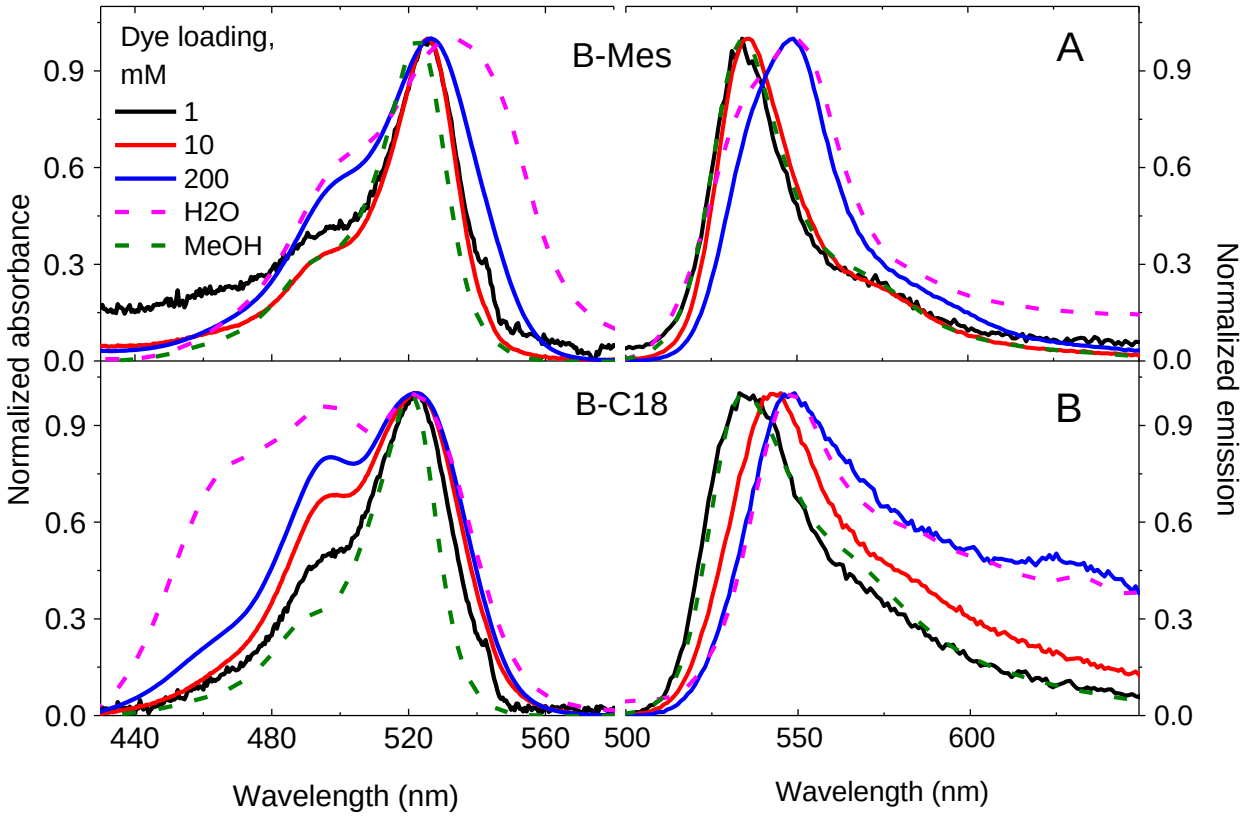

Figure 2. Normalized absorption (left) and fluorescence (right) spectra of PLGA NPs loaded with different amounts of B-Mes (A) and B-C18 (B) dyes, respectively, in 20 mM phosphate buffer (pH 7.4). For comparison, absorption and fluorescence spectra of B-Mes and B-C18 in water and methanol at concentration corresponding to 100 mM in PLGA are also shown.

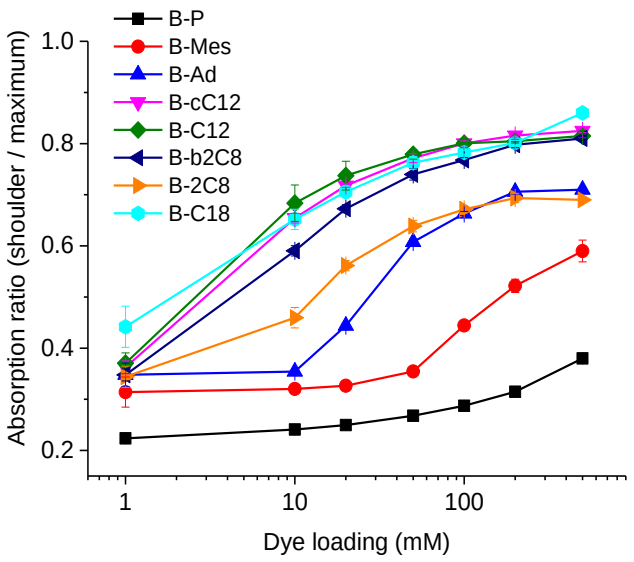

Figure 3. The ratio of the absorbance of the short-wavelength shoulder (500 nm for all dyes except or B-P: 475 nm) to the maximum for different BODIPY dyes inside PLGA NPs.

In neat water, all studied BODIPY dyes, except B-P showed very low values of fluorescence quantum yield (QY), clearly because of their strong aggregation (Fig. 4A). Co-precipitation of BODIPY dyes with PLGA strongly affected QY (Fig. 4B). At the lowest dye loading in PLGA NPs (< 10 mM), QY were high reaching for some dyes values close to 1 (Fig. 4A). Remarkably, for most of dyes these values exceeded those in methanol (0.4 - 0.6, Fig. 4B), suggesting that rigid polymer matrix minimizes non-radiative deactivation of the dyes. With increase in dye concentration in PLGA NPs, the QY values decreased gradually, showing that dye aggregation leads to poorly emissive species. Remarkably, the least hydrophobic B-P kept relatively high values of QY, so that at 500 mM loading, QY of B-P was ~0.27, very close to that in water. We could speculate that at the high dye loading B-P is not well encapsulated, so that its emission is similar to free molecular species dissolved in water. This is not the case for other dyes, where for most of loadings the QY values in PLGA NPs are higher than those in water.

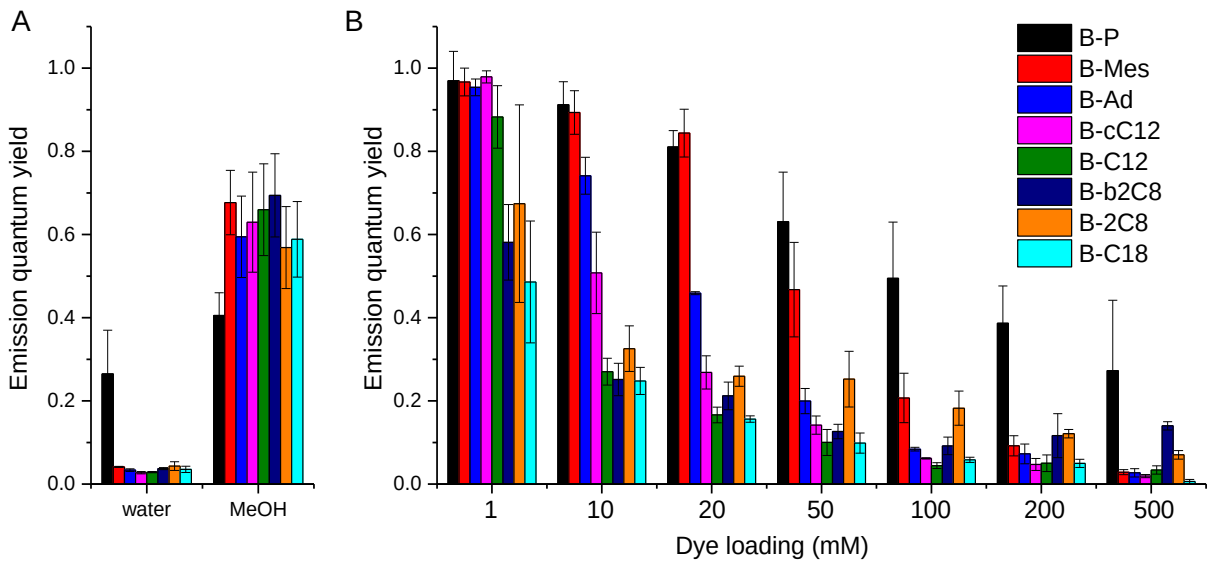

Figure 4. Fluorescence quantum yield of different BODIPY dyes in solvents (A) and in PLGA NPs at different dye loadings (B). Measurements in water and methanol without polymer were done at concentration corresponding 100 mM loading. Rhodamine 6G in EtOH was taken as a reference.

Further, we have modeled the biological environment to test the leakage of BODIPY dyes from the polymer particles by adding 10 % fetal bovine serum (FBS) to BODIPY (200 mM) NP solutions. The leakage of dyes was evaluated by fluorescence correlation spectroscopy (FCS) (Table 1).[64-66] FCS is a powerful tool to characterize NPs size[67] and polydipersity,[68] as well as to evaluate their behavior in biological media,[69] including their stability,[70, 71] and formation of protein corona on the surface of NPs.[72, 73] Recent studies showed the possibility to use FCS to study leakage of dyes from unilamellar lipid vesicles,[74] and lipid nano-droplets directly in biological media.[17, 75] In the latter studies, it was shown that dye leakage can be readily detected as an increase in the number of emissive species, because dyes, initially concentrated inside NPs, are spread all over the biological media. Without FBS most of the NPs showed a number of emissive species of 0.4-0.7 per excitation volume. The only exceptions were NPs prepared with B-Mes and especially B-P showing much larger number of emissive species, 2.0 and 14.2, respectively. The latter suggests that a significant fraction of these dyes are not encapsulated and free in solution, in line with our conclusions made for B-P based on spectroscopy data. Moreover, the quality of the fit of the auto-correlation curve was less good in case of B-P PLGA NPs in buffer, probably because of contribution from the non-encapsulated fraction of the dye (Fig. S5). For most NPs, addition of FBS induced a significant enhancement of signal intensity as well as large increase in the number of emissive species (3.6-26.9-fold, Table 1), except for NPs encapsulating B-C18 and B-2C8 dyes (only 1.8-fold). An increase in the number of emissive species in the detection volume is directly linked to the amount of free BODIPY dyes escaped from NPs due to interaction with FBS components (proteins and lipoproteins). On the other hand, the increase in overall average signal intensity of the sample in the presence of FBS is probably related to dyes that are initially quenched inside NPs and that enhance their emission once bound to the serum components. Again, this value was the largest for B-P, confirming very poor encapsulation of this dye into PLGA NPs. Importantly, in case of NPs prepared with B-C_{18} and B-$2C_8$, the fluorescence intensity did not change much in the presence of FBS, confirming that the dye leakage in these cases is minimal. The obtained results showed a clear correlation of the dye leakage with hydrophobicity of BODIPY dyes. Indeed, the highest stability against leakage is observed for the most hydrophobic dyes B-C18 and B-2C8 displaying the highest ClogP values (13.44, 14.75

respectively), despite of their quite different chemical structure. The first dye, B-C18, has the longest hydrophobic C18 chain, while the second, B-2C8, has two octyl chains. Surprisingly, even small shortening of the hydrophobic chain, as in the case of B-C12 (ClogP value 11.58), dramatically increased the leakage from NPs, showing the largest increase in signal intensity and the number of emissive species (Table 1). When comparing the dyes with two-branched chains, B-2C8 and B-b2C8, branching had a negative impact on the stability of NPs, as B-b2C_8 NPs showed much stronger changes in serum. Then, dyes with cyclic alkyl groups (B-cC12) showed similar poor resistance to leakage. Finally, dyes without any hydrophobic chain (B-P, B-Mes) showed dye leakage even in water and it was further enhanced by FBS. These dyes, being the least hydrophobic, showed the poorest encapsulation.

It should be also noted that the addition of FBS resulted in an increase in the hydrodynamic diameter (D) for most of NPs (Table 1). It is well known that when NPs come into contact with a biological fluid their surfaces are being covered with a "corona" of biological macromolecules, usually proteins, [72, 73, 76, 77] which naturally leads to an increase in NPs size. Interestingly, the largest increase in size (by 20-24 nm) was observed for B-C18 and B-2C8 dyes, i.e. for the most stable NPs (Table 1). This increase corresponds well to the thickness of protein corona (10-12 nm), which is within the range reported for different serum proteins (3-14 nm) adsorbed on quantum dots,[73] and similar to that reported for PLGA NPs in FBS.[48] For NPs loaded with other BODIPYs the increase in size was smaller and, in some cases, even decrease in size was observed (B-P, B-C12). The latter could be explained by strong leakage from these NPs, especially in the case of B-P and B-C12 loaded NPs, which shifted downward the apparent values of the NPs size.

Table 1. FCS parameters of PLGA NPs loaded with 200 mM BODIPY dyes before and after addition of 10 % FBS.[a]

Sample	Avg. signal [kHz]	n	τ_{diff} [ms]	cpp [kHz]	D [nm]	N_{ser}/n
Fluorescein	26.3±0.8	8.6±1.3	0.02±0	3.1±0.6	1±0	
B-C18	1.3±0.3	0.5±0.2	1.14±0.04	3±1.6	53±6	
B-C18 Serum	1.3±0.1	0.9±0.5	1.75±0.61	1.7±1.0	77±30	1.8±0.4
B-2C8	2.2±0.1	0.7±0.2	1.01±0.09	3.3±0.9	47±1	
B-2C8 Serum	2.6±0.3	1.3±0.6	1.52±0.51	2.4±1.4	67±27	1.8±0.4
B-b2C8	1.9±0.3	0.6±0.1	0.99±0.22	3.4±0.2	45±6	
B-b2C8 Serum	3.6±1.6	2.9±0.6	1.41±0.45	1.2±0.3	60±14	5.0±0.1
B-C12	2.1±0.4	0.5±0.1	0.96±0.16	4.1±0.6	44±4	
B-C12+Serum	14.2±6.5	14±2.3	0.69±0.07	1.0±0.3	30±1	26.9±4.2
B-cC12	3.4±0.3	0.4±0.1	1.08±0.09	9.7±1.9	50±1	
B-cC12 Serum	9.6±3.7	2.8±1.5	1.14±0.22	3.5±0.5	49±5	7.5±2.0
B-Ad	5.6±2	0.6±0.2	0.94±0.04	9.3±0.2	43±2	
B-Ad Serum	17.7±12	8.5±4.9	1.24±0.41	2.0±0.3	53±14	13.4±3.6
B-Mes	11.6±7.6	2.0±0.1	1.05±0.3	5.8±4.1	48±10	
B-Mes Serum	44.5±11.3	17.9±12.2	1.46±0.82	3.5±3.0	62±30	8.6±5.4
B-P	129±5	14.2±4.9	1.28±0.52	9.6±2.9	60±29	
B-P Serum	369±12	49.3±8.6	0.98±0.23	7.6±1.1	43±13	3.6±0.7

[a]n – number of emissive species per focal volume, t_{diff} – diffusion time, cpp – counts per particle, D – hydrodynamic diameter, n_{ser}/n – change in the emissive species number after addition of FBS. Excitation was 488 nm, while emission was collected through band-pass filter 525 / 50. Note that the excitation and signal collection for BODIPY NPs was much less efficient than for the dye reference fluorescein. In particular, due to the use quad-band (405/488/532/635) dichroic filter, a significant part of emission from BODIPY NPs (around 532 nm) was not collected.

FCS results were supported by time-laps studies of absorption (Fig. S6 I and III) and emission spectra (Fig. S6 II and IV, Fig. 5) of BODIPY NPs in a buffer and after addition of serum (FBS). Without FBS, absorption of BODIPY NPs (Fig. S6 III) showed negligible changes over time, while emission intensity decreased to a small extent (Fig. S6 IV, Fig. 5B). These results suggest that NPs are relatively stable over the studied time period. On the contrary, after addition of serum, emission intensity of all NPs, expect B-C18 and B-2C8 NPs, started and continued increasing for 24 h (Fig. 5 and S6). These results are in line with FCS data, suggesting that only B-C18 and B-2C8 NPs are stable in FBS, while all others undergo dye leakage to the biological environment. For most of leaky NPs, the release looked continuous over 24h with somewhat faster increase in the first 90 min. The fluorescence increase was especially strong B-C12, B-cC12 and B-Ad NPs (Fig. 5A), and it was accompanied by a decrease in the relative intensity of the shoulder corresponding to the aggregated dyes (Fig. S6 CI-FI). These dyes being aggregated and self-quenched within NPs probably partitioned to FBS in molecular form.

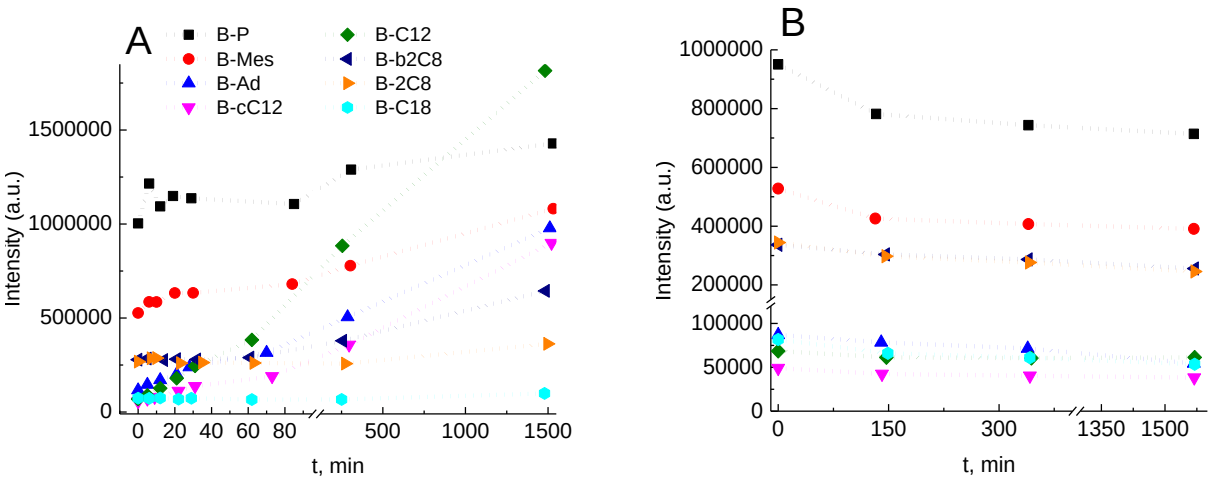

Figure 5. Time-dependent changes in emission intensity (at the maximum) of different BODIPY NPs (200 mM loading) after addition of 10 % FBS (A) and without FBS (B) in phosphate buffer (pH 7.4). λ_{ex} = 490 nm for all dyes, except B-P: λ_{ex} = 470 nm.

Finally, BODIPY-loaded NPs were incubated with HeLa cells and further studied by confocal microscopy (Fig. 6). After 2h incubation, an intensive and nearly homogeneous fluorescence all over the cytoplasm was observed for all BODIPY NPs, except those loaded with B-2C8 and B-C18 dyes. This homogeneous fluorescence inside the cells suggests that a significant fraction of the dye cargo was released from the particles and the free dye could readily distribute all over the cells. As these dyes are highly hydrophobic they probably stain intracellular membrane compartments of the cells. In sharp contrast, NPs loaded with B-2C8 and B-C18 displayed a granular pattern localized close to the nucleus, indicating that the dyes remained enclosed inside endosomes (Fig. 6). In the case of these NPs, negligible fluorescence in the cytoplasm of the cells was observed. This cell staining profile is in line with our

earlier studies on PLGA NPs loaded with Lumogen Red[48] and dye ions pairs[19, 24] that also did not exhibit any dye leakage. The observed results are in full accordance with the FCS data, showing that only NPs loaded with B-2C8 and B-C18 are resistant to dye leakage in biological media.

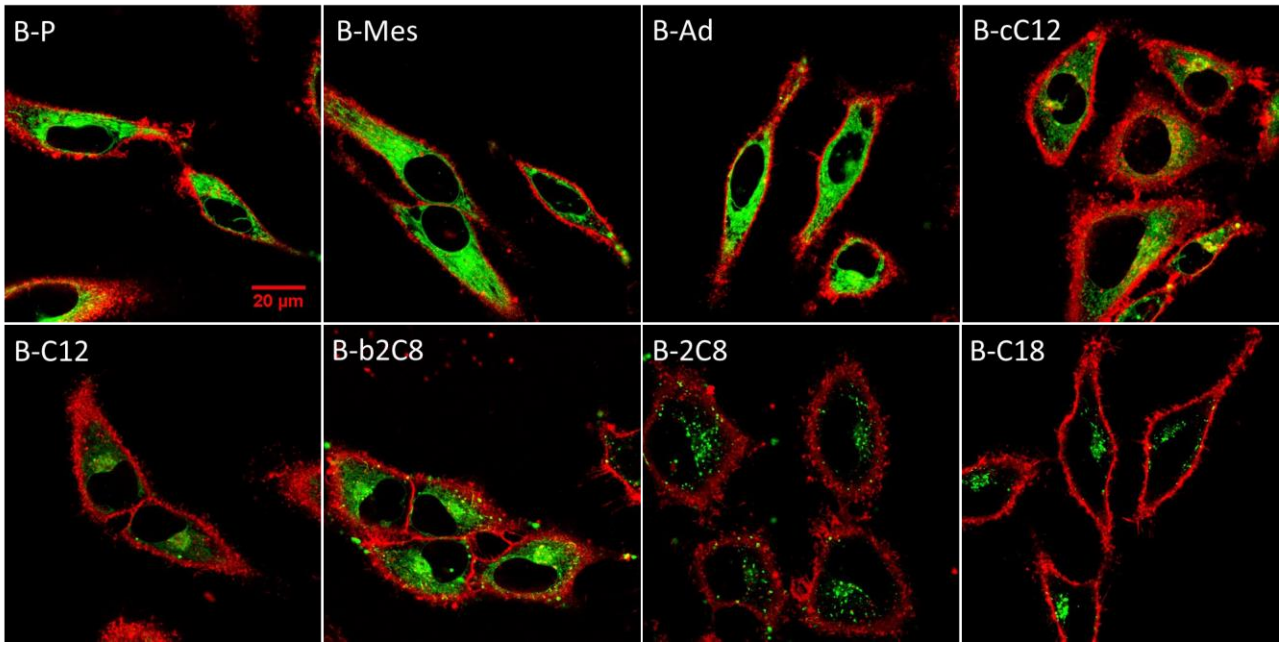

Figure 6. Confocal fluorescence imaging of HeLa cells incubated for 2 h with PLGA NPs loaded with different BODIPY dyes (200 mM dye loading) (green). Plasma membranes of the cells were stained with dSQ12S probe[78] (20 nM, 10 min incubation) (red).

Overall, our results highlight significance of the cargo hydrophobicity for efficient encapsulation inside polymeric NPs prepared by nanoprecipitation. Analysis of the loading efficiency by the filtration suggests that all the studied dyes, except the least hydrophobic B-P, are efficiency blended with the polymer NPs (Fig. 1C), whereas optical spectroscopy and microscopy data show strong variation in the dye leakage for these dyes as a function of their chemical structure (Table 1, Fig. 5 and 6). In our case, it is clear that only the most hydrophobic BODIPY derivatives (ClogP > 13) are capable to be encapsulated well into PLGA NPs showing no leakage in serum and living cells. On the one hand, it is clear that more hydrophobic dyes due to their higher LogP will have tendency to better partition into hydrophobic matrix and be less soluble in water. On the other hand, the problem is connected with the nanoprecipitation, which is a kinetically controlled process.[79-81] More hydrophobic molecules being less soluble in water should nanoprecipitate faster in aqueous media than more polar dyes. Therefore, during polymer nanoprecipitation the most hydrophobic BODIPY dyes may precipitate faster than or at least as fast as the polymer. This type of co-precipitation would result in efficient encapsulation (Scheme 2), where the dyes form a core of polymeric particle or at least distribute well inside the matrix of polymer NP. Indeed, we could show recently that such a core-shell structure is formed in the case of encapsulation of salts of rhodamine derivatives with hydrophobic counterions, and that it depends on the polymer hydrophobicity.[81] It was also shown that more hydrophobic counterions improved encapsulation of a rhodamine dye into PLGA NPs.[82]

However, less hydrophobic dyes may precipitate much slower than the polymer, which would lead first to formation of the polymer particle followed by adsorption of the dye on the particle surface (Scheme

2). This type of co-precipitation should lead to poor encapsulation and therefore to leakage in biological media, observed in our FCS, optical spectroscopy and cell imaging studies. In this respect, the differences between B-2C8 and B-b2C8 should be mentioned. Although these two dyes have very similar hydrophobicity and LogP, the branched structure of alkyl chains of B-b2C8 should significantly slow down its precipitation in aqueous media, leading to less efficient encapsulation prone to the dye leakage. Remarkably, as shown in our time-laps measurements (Fig. 5), the leakage is a relatively slow processes on the time scale of hours, probably because poorly encapsulated dyes still need to diffuse to the particle surface before being desorbed and transferred to components of serum (e.g. albumins and lipoproteins). We should stress that in our case the poor encapsulation does not mean inefficient loading, because BODIPYs of medium hydrophobicity can be efficiently loaded (blended) in PLGA NPs, but still leak to a large extent in biological media because of their shallow location within the particle (Scheme 2). Finally, we should note that most of the studied dyes except B-P are rather hydrophobic and poorly soluble in water. Therefore, their leakage cannot be observed in water, but requires a biological media, such as serum (Table 1) or cell membranes (Fig. 6) that could solubilize these dyes, driving the leakage of adsorbed or poorly encapsulated dyes. Our conclusions corroborate with previously reported observations for polymeric NPs.[19, 21] Indeed, Pegaz *et al.* showed that hydrophobicity of porphyrins is essential in obtaining stable polymeric NPs without dye leakage in cells.[21] Our recent works showed that stable NPs could be made either from highly hydrophobic perylene diimide dye (Lumogen Red)[48] or using hydrophobic cationic dyes with bulky hydrophobic counterions.[19, 24, 33, 82]

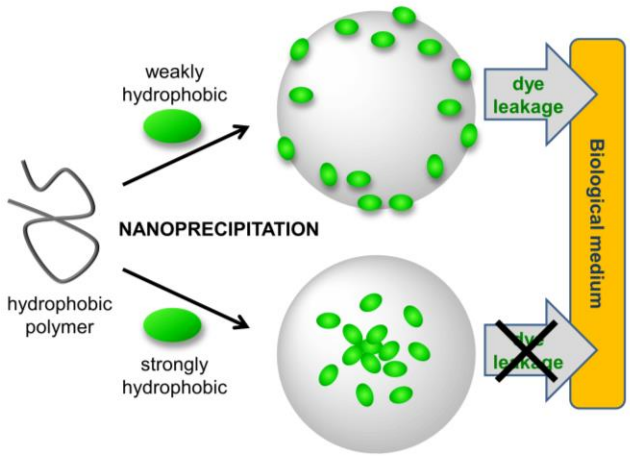

Scheme 2. Schematic presentation of nanoprecipitation of a hydrophobic polymer together with a fluorescent cargo of different hydrophobicity. It is illustrated that more hydrophobic cargos tend to be well encapsulated inside polymer NPs, while more polar molecules localize at the particle surface, which makes them prone to dye leakage.

Conclusions

Uncontrolled rapid release of cargo from polymeric nanoparticles constitutes a fundamental problem in the design of nanocarriers for drugs and contrast agents. Here, we investigated fluorescent dye-loaded PLGA NPs prepared by nanoprecipitation. As a cargo, we designed fluorescent BODIPY dyes of different polarity (calculated LogP), in order to understand the effect of cargo structure on the optical properties of NPs as well as on their stability against dye leakage (leaching). Spectroscopic studies showed that dye loading inside PLGA NPs has a profound effect on the formation of non-fluorescent

aggregates of dyes in the polymer matrix. Nevertheless, even at very high loading (200 mM with respect to the polymer), we could obtain NPs with acceptable fluorescence quantum yields of ~5-10%. Single-particle characterization by FCS revealed that in the presence of 10 % of FBS most of the BODIPY dyes leak from PLGA NPs, except BODIPY bearing long hydrophobic chain (octadecyl) B-C18 and two shorter chains (dioctyl) B-2C8. The extent of leakage decreased clearly with increase in the dye hydrophobicity (LogP). The time-laps absorption and fluorescence studies confirmed this result, revealing that the release kinetics for the leaky NPs is on the time scale of hours. Fluorescence microscopy of cells incubated with BODIPY NPs confirmed that only for B-C18 and B-2C8, presenting highest values of LogP, NPs remained stable inside the cells, being observed in form of bright endocytosed dots. By contrast, all other BODIPY NPs underwent significant dye leakage after incubation with cells, evidenced by a homogeneous fluorescence inside the cells. These results highlight an importance to avoid common misinterpretation of imaging data, where the observed fluorescence inside the cells does not necessarily mean the signal from internalized NPs, but rather emission of the dye cargo released from NPs. Moreover, the obtained results show that the nanoprecipitation protocol can provide efficient encapsulation of cargo into polymeric NPs only when the cargo is highly hydrophobic. We hypothesize that highly apolar dyes tend to form a core of highly concentrated dyes surrounded by a shell of nearly blank polymer, which prevents burst release from NPs. The present work provides new insights on the efficient cargo loading into polymeric NPs with minimal burst release based on a simple method of nanoprecipitation, which is important for development of fluorescent and drug-loaded nanomaterials.

Materials and methods

Materials

Poly(D,L-lactide-co-glycolide) (PLGA, lactide 50 mol %, glycolide 50 mol %, acid terminated, Mn 24 000, PDI 1.7, and Mn 8800, PDI 1.7) was purchased from Sigma-Aldrich and used as received. Sodium phosphate monobasic (>99.0%, Sigma-Aldrich) and sodium phosphate dibasic dihydrate (>99.0%, Sigma-Aldrich) were used to prepare 20 mM phosphate buffer solutions at pH 7.4. Tris(hydroxymethyl)aminomethane (Tris base, >99.8%, Sigma-Aldrich) and HCl (1 M) were used to prepare 20 mM Tris buffer with a pH of 7.4. Milli-Q water (Millipore) was used in all experiments. Membrane probe dSQ12S was synthesized as described before.[78]

Synthesis of BODIPY derivatives

B-P[83] and B-Mes[58] were synthesized according to a published protocols. NMR spectra were recorded at 20°C on Bruker Avance III 400MHz spectrometer. Mass spectra were obtained using an Agilent Q-TOF 6520 mass spectrometer.

Compound 1. A sealed tube in which was added glutaric anhydride (800 mg, 7.017 mmol), dioxane (4 mL) followed by 3-Ethyl-2,4-dimethylpyrrole (1.6 mL, 14.03 mmol, 2 eq) and $BF_3.OEt_2$ (1.6 mL, 10.52 mmol, 1.5 eq) was allowed to stir at 110°C for 1 hour before being cooled down to room temperature. The sealed tube was open and the solvents were evaporated. The crude was purified by column chromatography on silica gel (DCM/MeOH: 99/1 to 98/2) and crystallization (DCM/Heptane : 1/1) to

obtain 429 mg of **BODIPY-COOH** (16%) as a red solid. Rf=0.48 (DCM /MeOH, 95/5). ^{1}H-NMR (400 MHz, MeOD, $CHCl_3$): δ 3.15-3.10 (m, 2H, CH_2), 2.52 (t, *J* = 7.2 Hz, 2H, CH_2), 2.46 (m, 10H, 2CH2 Et, 2CH_3), 2.40 (s, 6H, 2 CH_3), 1.96-1.92 (m, 2H, CH_2), 1.08 (t, *J* = 7.6 Hz, 6H, CH_3 Et). ^{13}C NMR (101 MHz; MeOD, $CHCl_3$): δ 175.0 (CO), 151.9, 144.2, 136.1, 132.6, 130.8, 33.6, 27.2, 26.8, 16.6, 13.8, 12.3, 11.2. HRMS (ES+), calcd for $C_{21}H_{29}B\ F_2N_2NaO_2$ $[M+Na]^+$ 413.2188, found 413.2172.

General procedure for the synthesis of lipophilic BODIPYs. To a solution of BODIPY-COOH (20 mg, 0.051 mmol) in dry DMF (2 mL) was added the corresponding amine (1.5 eq) followed by HATU (23 mg, 0.062 mmol, 1.2 eq) and DIEA (27 μL, 0.153 mmol, 3 eq). The solution was allowed to stir at room temperature for 30 minutes. The solvents were evaporated and the products were purified by preparative thin layer chromatography (DCM 100%).

B-C12: 25 mg (86%) Rf=0.14 (DCM). ^{1}H-NMR (500 MHz, $CDCl_3$): δ 5.51 (t, *J* = 5.2 Hz, 1H, NH), 3.26 (q, *J* = 6.6 Hz, 2H), 3.08-3.05 (m, 2H), 2.51 (s, 6H, 2 Me), 2.41 (q, *J* = 7.6 Hz, 4H, CH_2 Et), 2.36-2.32 (m, 8H, 2 Me + CH_2), 2.00-1.96 (m, 2H), 1.50 (q, *J* = 7.1 Hz, 2H), 1.32-1.27 (m, 18H, CH2 C18), 1.06 (t, *J* = 7.6 Hz, 6H, CH3 Et), 0.90 (t, *J* = 7.0 Hz, 3H, CH3 C12). ^{13}C NMR (126 MHz; CDCl3): δ 171.5, 152.3, 143.7, 135.8, 132.7, 131.0, 39.7, 36.4, 31.9, 29.65, 29.63, 29.60, 29.55, 29.34, 29.31, 27.64, 27.48, 27.0, 22.7, 17.2, 14.8, 14.1, 13.4, 12.4. HRMS (ES+), calcd for $C_{33}H_{54}BF_2N_3NaO$ $[M+Na]^+$ 580.4226, found 580.4208.

B-C18: 21 mg (62%) Rf=0.23 (DCM). ^{1}H-NMR (500 MHz, $CDCl_3$): δ 5.54-5.51 (m, 1H, NH), 3.28-3.24 (m, 2H, CH_2), 3.08 (d, *J* = 5.2 Hz, 2H, CH_2), 2.52 (s, 6H, 2 CH_3), 2.41 (q, *J* = 7.6 Hz, 4H, 2 CH_2 Et), 2.36 (m, 8H, CH_2 + 2 CH_3), 2.00-1.97 (m, 2H, CH_2), 1.51 (t, *J* = 7.0 Hz, 2H, CH_2), 1.31 (d, *J* = 5.5 Hz, 32H, CH_2 C18), 1.06 (t, *J* = 7.6 Hz, 6H, CH_3 Et), 0.90 (t, *J* = 7.0 Hz, 3H, CH_3 C18). ^{13}C NMR (126 MHz; CDCl3): δ 171.6, 152.3, 143.7, 135.8, 132.7, 131.0, 39.7, 36.4, 31.9, 29.70, 29.68, 29.66, 29.64, 29.61, 29.56, 29.36, 29.31, 27.63, 27.48, 27.0, 22.7, 17.2, 14.8, 14.1, 13.4, 12.4. HRMS (ES+), calcd for $C_{39}H_{66}BF_2N_3NaO$ $[M+Na]^+$ 664.5165, found 664.5147.

B-Ad: 26 mg (94%) Rf=0.21 (DCM). ^{1}H-NMR (500 MHz, $CDCl_3$): δ 5.56-5.53 (m, 1H, NH), 3.73 (s, 2H, N-CH_2), 3.07 (dd, *J* = 10.1, 6.9 Hz, 2H), 2.98 (d, *J* = 6.3 Hz, 2H), 2.51 (s, 6H), 2.44-2.37 (m, 12H, 1 CH_2, 2 CH_2 Et, 2 CH_3), 1.99 (d, *J* = 9.7 Hz, 5H), 1.74 (d, *J* = 12.2 Hz, 3H), 1.64 (d, *J* = 11.4 Hz, 3H), 1.49 (d, *J* = 2.5 Hz, 6H), 1.06 (t, *J* = 7.6 Hz, 6H, 2 CH3 Et). ^{13}C NMR (126 MHz; $CDCl_3$): δ 171.8, 152.3, 143.7, 135.8, 132.7, 131.0, 67.1, 51.0, 40.3, 36.9, 36.6, 33.6, 28.2, 27.7, 27.5, 17.2, 14.8, 13.4, 12.4. HRMS (ES+), calcd for $C_{32}H_{46}BF_2N_3NaO$ $[M+Na]^+$ 560.3600, found 560.3575.

B-2C8: 30 mg (95%) Rf=0.34 (DCM). ^{1}H-NMR (500 MHz, $CDCl_3$): δ 3.31 (t, *J* = 7.7 Hz, 2H, CH_2), 3.22 (t, *J* = 7.8 Hz, 2H, CH_2), 3.11-3.08 (m, 2H, CH_2), 2.52 (s, 6H, 2 CH_3), 2.48 (t, *J* = 7.1 Hz, 2H, CH_2), 2.44-2.39 (m, 10H, 2 CH_3 + 2 CH_2 Et), 2.04-1.98 (m, 2H, CH_2), 1.54 (dt, *J* = 14.3, 7.0 Hz, 4H, 2 CH_2), 1.31 (t, *J* = 2.4 Hz, 20H), 1.06 (t, *J* = 7.6 Hz, 6H, 2 CH_3 Et), 0.91 (dt, *J* = 11.0, 7.0 Hz, 6H, 2 CH_3 C8). ^{13}C NMR (126 MHz; $CDCl_3$): δ 171.2, 152.2, 144.1, 135.8, 132.6, 131.1, 48.2, 46.1, 32.8, 31.82, 31.78, 29.41, 29.34, 29.24, 27.86, 27.78, 27.4, 27.10, 26.97, 22.64, 22.63, 17.2, 14.8, 14.1, 13.5, 12.41, 12.39. HRMS (ES+), calcd for $C_{37}H_{62}BF_2N_3NaO$ $[M+Na]^+$ 636.4852, found 636.4836.

B-b2C8: 28 mg (89%) Rf=0.46 (DCM). 1H-NMR (500 MHz, $CDCl_3$): δ 3.34 (ddd, *J* = 13.5, 7.8, 3.3 Hz, 1H, CH), 3.27 (ddd, *J* = 13.6, 7.0, 3.5 Hz, 1H, CH), 3.16 (d, *J* = 7.5 Hz, 2H, CH_2), 3.09-3.06 (m, 2H, CH_2), 2.52-2.49 (m, 8H, CH_2 + 2 CH_3), 2.44-2.39 (m, 10H, 2 CH_2 Et + 2 CH_3), 2.05-1.98 (m, 2H, CH_2), 1.70-1.60 (m, 2H), 1.29 (m, 16H, CH_2 C8), 1.06 (t, *J* = 7.6 Hz, 6H, 2 CH_3 Et), 0.94-0.87 (m, 12H, 4 CH_3 C8). 13-C NMR (126 MHz; $CDCl_3$): δ 172.1, 152.2, 144.0, 51.60, 51.59, 48.95, 48.93, 38.64,

38.64, 37.1, 33.2, 30.62, 30.58, 28.82, 28.74, 28.72, 27.9, 27.5, 23.91, 23.84, 23.10, 23.05, 17.2, 14.8, 14.07, 14.05, 13.5, 12.43, 12.41, 12.39, 10.86, 10.85, 10.69, 10.68. HRMS (ES+), calcd for $C_{37}H_{62}BF_2N_3NaO$ [M+Na]+ 636.4852, found 636.4827.

B-cC12: 27 mg (98 %) Rf=0.32 (DCM). ^{1}H-NMR (500 MHz, $CDCl_3$): δ 5.31 (d, *J* = 8.5 Hz, 1H, NH), 4.11-4.08 (m, 1H, CH C_{12}), 3.07 (dt, *J* = 7.6, 4.2 Hz, 2H, CH_2), 2.51 (s, 6H, 2 CH_3), 2.41 (q, *J* = 7.6 Hz, 4H, 2 CH_2 Et), 2.36 (s, 6H, 2 CH_3), 2.32 (t, *J* = 7.2 Hz, 2H, CH_2), 2.01-1.95 (m, 2H, CH_2), 1.62 (m, 2H), 1.49-1.36 (m, 20H, CH2 C_{12}), 1.06 (t, *J* = 7.6 Hz, 6H, 2 CH_3 Et). ^{13}C NMR (126 MHz; $CDCl_3$): δ 170.8, 152.3, 143.7, 135.8, 132.7, 131.0, 46.2, 36.7, 30.3, 27.66, 27.59, 24.0, 23.7, 23.48, 23.33, 21.4, 17.2, 14.8, 13.4, 12.43, 12.41. HRMS (ES+), calcd for $C_{33}H_{52}BF_2N_3NaO$ $[M+Na]^+$ 578.4069, found 578.4056.

NPs preparation

Stock solutions of PLGA (10 mg/ml) and BODIPY dyes (1 mM) were prepared in acetonitrile. PLGA solution was further diluted to 2 mg/ml with acetonitrile containing different concentration of BODIPY dyes corresponding to 1 to 200 mM loading with respect to the polymer. The molar concentration of dye in the polymer NPs was expressed with respect to the polymer, assuming polymer density of 1 g/ml. These polymer-dye solutions under stirring (shaking) were added quickly by a micropipette to a tenfold volume excess of 20 mM phosphate buffer at pH 7.4 (21 °C). The particle solution was then quickly diluted five-fold with the same buffer and then used directly in further studies. All dye loadings mentioned in the present study were calculated based on the initial (feeding) dye/polymer ratios.

For estimating the loading efficiency of BODIPY dyes in PLGA NPs, BODIPY-loaded PLGA NPs (200 mM dye loading) in buffer were first filtered through PTFE filter with pore size 0.20 µm (Rotilabo ® syringe filter) and then the filtrate was diluted 20 times in dioxane. The loading efficiency was calculated as the ratio of BODIPY absorbance after (A_f) and before (A_0) filtration measured in dioxane: $A_f/A_0 \times 100\%$. For comparison, NPs of BODIPY dyes without PLGA were prepared, filtrated and then analyzed similarly.

Characterization of NPs

Dynamic light scattering (DLS) measurements were performed on a Zetasizer Nano series DTS 1060 (Malvern Instruments S.A.). It uses a laser source at 633 nm, which excludes any light excitation of our dye-doped NPs. The Zetasizer software provided with standard cumulants and size distribution by volume analysis was used to characterize nanoparticles by DLS. For the data analysis the following parameters were used for the solvent (water) - temperature T 25°C, refractive index RI 1.33, viscosity 0.8872 cP. For the distribution analysis of correlation function a non-negative least squares algorithm was applied. Nanoparticles were assumed to be all homogenous and spherical in shape. Absorption and emission spectra were recorded on a Cary 4000 scan UV-visible spectrophotometer (Varian) and a FluoroMax-4 spectrofluorometer (Horiba Jobin Yvon) equipped with a thermostated cell compartment, respectively. For standard recording of fluorescence spectra, the excitation wavelength was set to 485 nm, unless indicated. The fluorescence spectra were corrected for detector response and lamp fluctuations. Fluorescence quantum yields were calculated using rhodamine 6G in ethanol (QY = 0.95) as a reference with an absorbance of 0.01 at (520 nm).

FCS measurements were acquired on a home-build setup based on a Nikon Ti-E inverted microscope. For sample excitation we have used the module of 488 nm diode laser (Oxxius, France) guided through

the fiber optics and focused inside the sample with a water immersion objective (100X, NA=1.2). For the fluorescence signal detection, fibered Avalanche Photodiode (APD, Perkin-Elmer, Fremont, CA) was used. Before the APD, the fluorescence signal was filtered through 405/488/532/635 nm BrightLine® quad-edge laser-grade dichroic (Semrock, NY) and ET525 /50 single band-pass filter (Chroma Corp., Rockingham, VT). The fluorescence signal was further processed by an ALV7002/USB digital correlator (ALV, Langen, Germany). For FCS data analysis we have used PyCorrFit free software created by Muller et al.[84] To calculate the size and concentration of NPs, 50 nM solution fluorescein (TRIS, pH 9) was used as a reference. In case of 10% FBS, the change in the viscosity (0.94 cP in 10% FBS vs. 0.88 cP in water at 25°C)[85] was taken into account in the calculation of size of NPs.

Cellular experiments

HeLa cells (ATCC® CCL-2) were grown in Dulbecco's modified Eagle's medium (DMEM, Gibco-Invitrogen), supplemented with 10% fetal bovine serum (FBS, Lonza) and 1% antibiotic solution (penicillin–streptomycin, Gibco-Invitrogen) at 37 °C in a humidified atmosphere containing 5%CO2. Cells were seeded onto a chambered coverglass (IBiDi) at a density of 5×10^4 cells per well 24 h before the microscopy measurement. For imaging, the culture medium was removed and the attached cells were washed with Opti-MEM (Gibco-Invitrogen). Then, a freshly prepared solution of NPs (at 20-fold dilution of the original formulation corresponding to ~0.15 nM of NPs) in Opti-MEM was added to the cells and incubated for 2 hours. Cell membrane staining with dSQ12S 20 nM was done for 10 min at rt before the measurements. Confocal fluorescence images of the cells were taken on a Leica TSC SPE confocal microscope using a 63× oil immersion objective. The different channels were recorded as follows: (i) for BODIPY NPs, excitation 488 nm, emission from 495 to 560 nm; (ii) for dSQ12S, excitation 635 nm, emission from 650 to 750 nm.

Acknowledgements

This work was supported by the European Research Council ERC Consolidator grant BrightSens 648528. The authors thank to P. Didier for help in the installation of the FCS setup and R. Vauchelles from PIQ imaging platform.

Conflicts of interest

There are no conflicts of interest to declare.

References

1. L. Zhang, F. X. Gu, J. M. Chan, A. Z. Wang, R. S. Langer and O. C. Farokhzad, *Clin. Pharmacol. Ther.*, 2008, **83**, 761-769.
2. T. M. Sun, Y. S. Zhang, B. Pang, D. C. Hyun, M. X. Yang and Y. N. Xia, *Angew. Chem.-Int. Edit.*, 2014, **53**, 12320-12364.
3. T. L. Doane and C. Burda, *Chem. Soc. Rev.*, 2012, **41**, 2885-2911.
4. R. H. Prabhu, V. B. Patravale and M. D. Joshi, *Int. J. Nanomed.*, 2015, **10**, 1001-1018.

5. F. Masood, *Mater. Sci. Eng. C-Mater. Biol. Appl.*, 2016, **60**, 569-578.

6. A. Kumari, S. K. Yadav and S. C. Yadav, *Colloids and Surfaces B-Biointerfaces*, 2010, **75**, 1-18.

7. J. K. Vasir and V. Labhasetwar, *Advanced Drug Delivery Reviews*, 2007, **59**, 718-728.

8. A. Mahapatro and D. K. Singh, *J. Nanobiotechnol.*, 2011, **9**.

9. C. R. de Azevedo, M. von Stosch, M. S. Costa, A. M. Ramos, M. M. Cardoso, F. Danhier, V. Preat and R. Oliveira, *Int. J. Pharm.*, 2017, **532**, 229-240.

10. X. Huang and C. S. Brazel, *Journal of Controlled Release*, 2001, **73**, 121-136.

11. S. Behzadi, V. Serpooshan, R. Sakhtianchi, B. Muller, K. Landfester, D. Crespy and M. Mahmoudi, *Colloids and Surfaces B-Biointerfaces*, 2014, **123**, 143-149.

12. S. Mura, D. T. Bui, P. Couvreur and J. Nicolas, *J Control Release*, 2015, **208**, 25-41.

13. J. Rautio, H. Kumpulainen, T. Heimbach, R. Oliyai, D. Oh, T. Jarvinen and J. Savolainen, *Nat Rev Drug Discov*, 2008, **7**, 255-270.

14. O. I. Corrigan and X. Li, *European Journal of Pharmaceutical Sciences*, 2009, **37**, 477-485.

15. F. M. Helaly, H. S. M. Soliman, A. D. Soheir and A. A. Ahmed, *Adv Polym Tech*, 2001, **20**, 305-311.

16. A. J. Thote, J. T. Chappell, R. B. Gupta and R. Kumar, *Drug Dev. Ind. Pharm.*, 2005, **31**, 43-57.

17. A. S. Klymchenko, E. Roger, N. Anton, H. Anton, I. Shulov, J. Vermot, Y. Mely and T. F. Vandamme, *Rsc Advances*, 2012, **2**, 11876-11886.

18. S. Snipstad, S. Hak, H. Baghirov, E. Sulheim, Y. Morch, S. Lelu, E. von Haartman, M. Back, K. P. R. Nilsson, A. S. Klymchenko, C. D. Davies and A. K. O. Aslund, *Cytometry Part A*, 2017, **91A**, 760-766.

19. B. Andreiuk, A. Reisch, V. G. Pivovarenko and A. S. Klymchenko, *Materials Chemistry Frontiers*, 2017, **1**, 2309-2316.

20. H. T. Chen, S. W. Kim, L. Li, S. Y. Wang, K. Park and J. X. Cheng, *P Natl Acad Sci USA*, 2008, **105**, 6596-6601.

21. B. Pegaz, E. Debefve, F. Borle, J. P. Ballini, H. van den Bergh and Y. N. Kouakou-Konan, *Journal of Photochemistry and Photobiology B-Biology*, 2005, **80**, 19-27.

22. C. Simonsson, G. Bastiat, M. Pitorre, A. S. Klymchenko, J. Bejaud, Y. Mely and J. P. Benoit, *Eur. J. Pharm. Biopharm.*, 2016, **98**, 47-56.

23. T. Tenuta, M. P. Monopoli, J. Kim, A. Salvati, K. A. Dawson, P. Sandin and I. Lynch, *PLoS One*, 2011, **6**, 6.

24. B. Andreiuk, A. Reisch, M. Lindecker, G. Follain, N. Peyrieras, J. G. Goetz and A. S. Klymchenko, *Small*, 2017, **13**.

25. A. Reisch and A. S. Klymchenko, *Small*, 2016, **12**, 1968-1992.

26. K. Li and B. Liu, *Chem. Soc. Rev.*, 2014, **43**, 6570-6597.

27. X. Michalet, F. F. Pinaud, L. A. Bentolila, J. M. Tsay, S. Doose, J. J. Li, G. Sundaresan, A. M. Wu, S. S. Gambhir and S. Weiss, *Science*, 2005, **307**, 538-544.

28. A. P. Alivisatos, *Science*, 1996, **271**, 933-937.

29. J. E. Lee, N. Lee, T. Kim, J. Kim and T. Hyeon, *Accounts Chem. Res.*, 2011, **44**, 893-902.

30. S. Bonacchi, D. Genovese, R. Juris, M. Montalti, L. Prodi, E. Rampazzo and N. Zaccheroni, *Angew. Chem. Int. Ed.*, 2011, **50**, 4056-4066.

31. A. Wagh, F. Jyoti, S. Mallik, S. Qian, E. Leclerc and B. Law, *Small (Weinheim an Der Bergstrasse, Germany)*, 2013, **9**, 2129-2139.

32. A. Wagh, S. Y. Qian and B. Law, *Bioconjugate Chem.*, 2012, **23**, 981-992.

33. A. Reisch, P. Didier, L. Richert, S. Oncul, Y. Arntz, Y. Mely and A. S. Klymchenko, *Nature Communications*, 2014, **5**, 4089.

34. K. Hoffmann, T. Behnke, M. Grabolle and U. Resch-Genger, *Anal Bioanal Chem*, 2014, **406**, 3315-3322.

35. Z. Wang, S. Chen, J. W. Y. Lam, W. Qin, R. T. K. Kwok, N. Xie, Q. Hu and B. Z. Tang, *Journal of the American Chemical Society*, 2013, **135**, 8238-8245.

36. R. Ferrari, M. Lupi, F. Falcetta, P. Bigini, K. Paolella, F. Fiordaliso, C. Bisighini, M. Salmona, M. D'Incalci, M. Morbidelli, D. Moscatelli and P. Ubezio, *Nanotechnology*, 2014, **25**.

37. X. Diao, W. Li, J. Yu, X. Wang, X. Zhang, Y. Yang, F. An, Z. Liu and X. Zhang, *Nanoscale*, 2012, **4**, 5373-5377.

38. K. Li, Y. Jiang, D. Ding, X. Zhang, Y. Liu, J. Hua, S.-S. Feng and B. Liu, *Chem. Commun.*, 2011, **47**, 7323-7325.

39. K. Trofymchuk, A. Reisch, P. Didier, F. Fras, P. Gilliot, Y. Mely and A. S. Klymchenko, *Nature Photonics*, 2017, **11**, 657-663.

40. P. Mascalchi, E. Haanappel, K. Carayon, S. Mazeres and L. Salome, *Soft Matter*, 2012, **8**, 4462-4470.

41. N. Melnychuk and A. S. Klymchenko, *Journal of the American Chemical Society*, 2018, **140**, 10856-10865.

42. J. H. Na, H. Koo, S. Lee, K. H. Min, K. Park, H. Yoo, S. H. Lee, J. H. Park, I. C. Kwon, S. Y. Jeong and K. Kim, *Biomaterials*, 2011, **32**, 5252-5261.

43. A. Schädlich, H. Caysa, T. Mueller, F. Tenambergen, C. Rose, A. Göpferich, J. Kuntsche and K. Mäder, *ACS nano*, 2011, **5**, 8710-8720.

44. K. Kim, J. H. Kim, H. Park, Y. S. Kim, K. Park, H. Nam, S. Lee, J. H. Park, R. W. Park, I. S. Kim, K. Choi, S. Y. Kim and I. C. Kwon, *Journal of Controlled Release*, 2010, **146**, 219-227.

45. Y. Yang, X. Song, Y. Yao, H. Wu, J. Liu, Y. Zhao, M. Tan and Q. Yang, *J. Mater. Chem. B*, 2015, **3**, 4671-4678.

46. Y. N. Hong, J. W. Y. Lam and B. Z. Tang, *Chem. Soc. Rev.*, 2011, **40**, 5361-5388.

47. Z. Tian, A. D. Shaller and A. D. Q. Li, *Chem. Commun.*, 2009, DOI: 10.1039/b815507k, 180-182.

48. K. Trofymchuk, A. Reisch, I. Shulov, Y. Mely and A. S. Klymchenko, *Nanoscale*, 2014, **6**, 12934-12942.

49. I. Shulov, S. Oncul, A. Reisch, Y. Arntz, M. Collot, Y. Mely and A. S. Klymchenko, *Nanoscale*, 2015, **7**, 18198-18210.

50. A. Salvati, C. Aberg, T. dos Santos, J. Varela, P. Pinto, I. Lynch and K. A. Dawson, *Nanomed.-Nanotechnol. Biol. Med.*, 2011, **7**, 818-826.

51. A. Loudet and K. Burgess, *Chem. Rev.*, 2007, **107**, 4891-4932.

52. G. Ulrich, R. Ziessel and A. Harriman, *Angew. Chem.-Int. Edit.*, 2008, **47**, 1184-1201.

53. A. Fraix, M. Blangetti, S. Guglielmo, L. Lazzarato, N. Marino, V. Cardile, A. C. E. Graziano, I. Manet, R. Fruttero, A. Gasco and S. Sortino, *ChemMedChem*, 2016, **11**, 1371-1379.

54. R. Zagami, G. Sortino, E. Caruso, M. C. Malacarne, S. Banfi, S. Patanè, L. Monsù Scolaro and A. Mazzaglia, *Langmuir*, 2018, **34**, 8639-8651.

55. Q. Y. Tang, W. L. Si, C. H. Huang, K. K. Ding, W. Huang, P. Chen, Q. Zhang and X. C. Dong, *J. Mater. Chem. B*, 2017, **5**, 1566-1573.

56. L. Liu, L. Y. Fu, T. T. Jing, Z. Ruan and L. F. Yang, *Acs Applied Materials & Interfaces*, 2016, **8**, 8980-8990.

57. Z. Y. Wang, X. H. Hong, S. F. Zong, C. Q. Tang, Y. P. Cui and Q. D. Zheng, *Sci Rep*, 2015, **5**, 10.

58. R. Meallet-Renault, A. Herault, J. J. Vachon, R. B. Pansu, S. Amigoni-Gerbier and C. Larpent, *Photochemical & Photobiological Sciences*, 2006, **5**, 300-310.

59. A. Reisch, A. Runser, Y. Arntz, Y. Mély and A. S. Klymchenko, *ACS Nano*, 2015, **9**, 5104-5116.

60. H. Fessi, F. Puisieux, J. P. Devissaguet, N. Ammoury and S. Benita, *Int J Pharm*, 1989, **55**, R1-R4.

61. E. Genin, Z. H. Gao, J. A. Varela, J. Daniel, T. Bsaibess, I. Gosse, L. Groc, L. Cognet and M. Blanchard-Desce, *Adv. Mater.*, 2014, **26**, 2258-2261.

62. J. Mei, N. L. C. Leung, R. T. K. Kwok, J. W. Y. Lam and B. Z. Tang, *Chem. Rev.*, 2015, **115**, 11718-11940.

63. T. T. Vu, S. Badré, C. Dumas-Verdes, J.-J. Vachon, C. Julien, P. Audebert, E. Y. Senotrusova, E. Y. Schmidt, B. A. Trofimov, R. B. Pansu, G. Clavier and R. Méallet-Renault, *The Journal of Physical Chemistry C*, 2009, **113**, 11844-11855.

64. O. Krichevsky and G. Bonnet, *Rep. Prog. Phys.*, 2002, **65**, 251-297.

65. S. T. Hess, S. H. Huang, A. A. Heikal and W. W. Webb, *Biochemistry*, 2002, **41**, 697-705.

66. D. Woll, *Rsc Advances*, 2014, **4**, 2447-2465.

67. S. Dominguez-Medina, S. S. Chen, J. Blankenburg, P. Swanglap, C. F. Landes and S. Link, in *Annual Review of Physical Chemistry, Vol 67*, eds. M. A. Johnson and T. J. Martinez, 2016, vol. 67, pp. 489-514.

68. N. Pal, S. D. Verma, M. K. Singh and S. Sen, *Analytical Chemistry*, 2011, **83**, 7736-7744.

69. T. Liedl, S. Keller, F. C. Simmel, J. O. Radler and W. J. Parak, *Small*, 2005, **1**, 997-1003.

70. A. Reisch, A. Runser, Y. Arntz, Y. Mely and A. S. Klymchenko, *ACS Nano*, 2015, **9**, 5104-5116.

71. R. Bouchaala, N. Anton, H. Anton, T. Vandamme, J. Vermot, D. Smail, Y. Mely and A. S. Klymchenko, *Colloids and Surfaces B-Biointerfaces*, 2017, **156**, 414-421.

72. P. Del Pino, B. Pelaz, Q. Zhang, P. Maffre, G. U. Nienhaus and W. J. Parak, *Materials Horizons*, 2014, **1**, 301-313.

73. Y. Klapper, P. Maffre, L. Shang, K. N. Ekdahl, B. Nilsson, S. Hettler, M. Dries, D. Gerthsen and G. U. Nienhaus, *Nanoscale*, 2015, **7**, 9980-9984.

74. K. Kristensen, J. R. Henriksen and T. L. Andresen, *Biochimica Et Biophysica Acta-Biomembranes*, 2014, **1838**, 2994-3002.

75. R. Bouchaala, L. Richert, N. Anton, T. F. Vandamme, S. Djabi, Y. Mely and A. S. Klymchenko, *ACS Omega*, 2018, **3**, 14333-14340.

76. T. Cedervall, I. Lynch, S. Lindman, T. Berggard, E. Thulin, H. Nilsson, K. A. Dawson and S. Linse, *P Natl Acad Sci USA*, 2007, **104**, 2050-2055.

77. M. Lundqvist, J. Stigler, T. Cedervall, T. Berggard, M. B. Flanagan, I. Lynch, G. Elia and K. Dawson, *Acs Nano*, 2011, **5**, 7503-7509.

78. M. Collot, R. Kreder, A. L. Tatarets, L. D. Patsenker, Y. Mely and A. S. Klymchenko, *Chem. Commun.*, 2015, **51**, 17136-17139.

79. D. Horn and J. Rieger, *Angew. Chem.-Int. Edit.*, 2001, **40**, 4331-4361.

80. J. P. Rao and K. E. Geckeler, *Progress in Polymer Science*, 2011, **36**, 887-913.

81. A. Reisch, K. Trofymchuk, A. Runser, G. Fleith, M. Rawiso and A. S. Klymchenko, *ACS Appl. Mater. Interfaces*, 2017, **9**, 43030-43042.

82. B. Andreiuk, A. Reisch, E. Bernhardt and A. S. Klymchenko, *Chemistry – An Asian Journal*, 2019, **10.1002/asia.201801592**.

83. A. Vazquez-Romero, N. Kielland, M. J. Arevalo, S. Preciado, R. J. Mellanby, Y. Feng, R. Lavilla and M. Vendrell, *Journal of the American Chemical Society*, 2013, **135**, 16018-16021.

84. P. Muller, P. Schwille and T. Weidemann, *Bioinformatics*, 2014, **30**, 2532-2533.

85. E. Frohlich, G. Bonstingl, A. Hofler, C. Meindl, G. Leitinger, T. R. Pieber and E. Roblegg, *Toxicology in Vitro*, 2013, **27**, 409-417.